A novel defined cuproptosis-related signature score to predict prognosis and immunotherapy efficacy in pancreatic cancer

WEIYU GE[1,2], YONGCHAO WANG[2], DAIYUAN SHENTU[2], MING YUE[2] and YANLING WANG[2]

[1]Department of Medical Oncology, Fudan University Shanghai Cancer Center, Shanghai Medical College, Fudan University, Shanghai 200032, P.R. China; [2]State Key Laboratory of Oncogenes and Related Genes, Shanghai Cancer Institute, Department of Oncology, Renji Hospital, School of Medicine, Shanghai Jiao Tong University, Shanghai 200127, P.R. China

Received May 15, 2025; Accepted September 10, 2025

DOI: 10.3892/ol.2025.15337

Abstract. Cuproptosis, a novel mode of copper-dependent programmed cell death, represents a distinct mechanism separate from other established forms of cell death. The present study aimed to explore the intertumoral heterogeneity of cell death and its relationship with the tumor microenvironment (TME) in pancreatic cancer (PC). Multiple bioinformatics approaches, using multi-omics data from The Cancer Genome Atlas, Genome Tissue Expression, International Cancer Genome Consortium, Gene Expression Omnibus and Clinical Proteomic Tumor Analysis Consortium datasets, and *in vitro* validation were employed to comprehensively analyze the expression profile, prognostic value and immune cell infiltration of cuproptosis-related genes (CGs) in PC. The enrichment scores of five reported cell death modes were assessed by single-sample gene set enrichment analysis. The results revealed that cuproptosis exhibited the only protective effect on survival compared with other cell death modes and CDK inhibitor 2A was the core gene involved in PC cuproptosis status. The present study also evaluated the alterations in genomic backgrounds and the expression of CGs, and detected dysregulated mRNA levels, cell-free DNA levels and protein levels of CGs in PC. Subsequently, two distinct cuproptosis subtypes (CG cluster A and CG cluster B) were identified, and the potential roles of CGs in the TME, clinical features and immunotherapy response were delineated. Notably, it was observed that CG cluster B was associated with poor survival, stromal activation, immunosuppression and immunotherapy resistance in patients with PC. Furthermore, a highly accurate nomogram was developed to enhance the clinical applicability of the cuproptosis-associated risk score. A high-risk score, characterized by an increased mutation burden and stromal activation, was associated with worse survival. Furthermore, compared with the low-risk score group, a higher anti-programmed cell death protein-1 resistant-related signature was observed in the high-risk score group. These findings define a novel prognostic cuproptosis-related signature for the prediction of clinical outcomes and immunotherapy response in PC.

Correspondence to: Dr Weiyu Ge, Department of Medical Oncology, Fudan University Shanghai Cancer Center, Shanghai Medical College, Fudan University, 270 Dongan Road, Xuhui, Shanghai 200032, P.R. China
E-mail: geweiyu.com@sjtu.edu.cn; 1051394109@qq.com

Key words: cuproptosis, tumor immune microenvironment, prognosis, immunotherapy, pancreatic cancer

Introduction

Pancreatic cancer (PC) is characterized by high fatality rates, with a 5-year survival rate of ~4% (1,2). Notably, targeted therapies have proven inadequate, due to the substantial heterogeneity within PC (3). In recent years, immunotherapy has offered potential for the treatment of various solid tumors, including melanoma, lung cancer, breast cancer, renal cell carcinoma, head and neck cancer, esophageal cancer and bladder cancer (4,5); however, prior studies have suggested that unselected patients with PC often exhibit minimal or no response to immunotherapy (6-8).

Cell death mechanisms serve pivotal roles in maintaining physiological homeostasis, eliminating damaged cells and responding to pathological stimuli (9). Traditionally, apoptosis was considered the primary form of programmed cell death; however, recent advancements in tumor cell biology have identified various subtypes of programmed cell death, such as necroptosis, pyroptosis and ferroptosis, each associated with distinct biological contexts (10,11). Copper ions are indispensable for cellular physiology, including energy metabolism, mitochondrial respiration and antioxidant activity (12,13). Dysregulation of copper ions can disturb lipid metabolism, and one distinctive form of cell death, known as cuproptosis, emerges due to copper excess, resulting in oxidative stress, mitochondrial damage and endothelial cell dysfunction (14-16). In addition, recent research has revealed a novel mechanism of copper-induced cell death involving the aggregation of lipoylated dihydrolipoamide S-acetyltransferase (DLAT), a component of the mitochondrial tricarboxylic acid cycle, ultimately leading to proteotoxic stress and cell death termed cuproptosis (17,18). Mounting evidence has suggested that disrupted copper homeostasis can impact tumor growth (19-21), and targeted cuproptosis therapy holds

promise, particularly for highly fatal tumors with limited therapeutic options, such as PC (22,23). In the past decade, research into programmed cell death in tumors has indicated the immunogenicity of the tumor microenvironment (TME), rendering it amenable to anticancer interventions (24-26). Notably, various TME components undergoing programmed cell death can elicit immune responses against tumor cells, thereby enhancing antitumor effects. For example, tumor destruction facilitates antigen acquisition by conventional dendritic cells, promotes the recruitment of myeloid cells and restricts T-cell cytotoxic activity (27-29).

The latest research has suggested a novel connection between TME composition, cancer-associated fibroblasts (CAFs) and malignant cell stemness, as well as patient survival, which may lead to improved upfront risk stratification and more personalized clinical decision-making (30,31). Some studies have demonstrated the role of cuproptosis in tumorigenesis, tumor progression and prognosis (19,32). However, the unique molecular signature of cuproptosis and its interplay with the TME remain unexplored in PC. Therefore, investigating whether cuproptosis alters the TME and impacts anticancer therapy outcomes is a key research avenue.

The present study provides a comprehensive analysis of the difference in expression of cuproptosis-related genes (CGs) and gene variation, focusing on their latent roles in PC tumorigenesis, prognosis, TME and treatment outcomes using multi-omics data. Two distinct cuproptosis-related subtypes within PC were identified, and their molecular characteristics, prognostic significance and interactions with the tumor immune microenvironment were evaluated. Furthermore, a CG scoring system was established to predict clinical outcomes and immunotherapy responses in patients with PC. In conclusion, the present study established a risk score as a robust prognostic indicator for patients with PC, offering potential for precise risk stratification, insights into TME characteristics and the exploration of more effective immunotherapy strategies.

Materials and methods

PC data sources and preprocessing. The present study used multi-omics data from cohorts of patients with PC extracted from The Cancer Genome Atlas (TCGA), Genome Tissue Expression (GTEx), International Cancer Genome Consortium (ICGC), Gene Expression Omnibus (GEO), the Human Protein Atlas (HPA) and Clinical Proteomic Tumor Analysis Consortium (CPTAC) databases. The normalized mRNA expression data and corresponding clinical information from 160 patients with pancreatic adenocarcinoma (PAAD), including survival status, grade, sex and age, were obtained from TCGA (https://portal.gdc.cancer.gov/). Furthermore, another independent cohort was retrieved from the ICGC database (https://dcc.icgc.org/, which contained 101 PAAD cases. Samples from patients with a deficiency of clinical information were excluded from subsequent analysis. In addition, transcriptome data from 167 normal pancreatic tissues were downloaded from the public database GTEx project (https://www.gtexportal.org; gtex_RSEM_gene_fpkm).

Cell-free DNA data from liquid biopsies were obtained from the GEO (https://www.ncbi.nlm.nih.gov/geo/) database. Two GEO datasets containing 47 blood plasma samples of PC were included in the analysis, namely GSE136651 [normal=22 vs. tumor=10] (33) and GSE81314 (34) (normal=8 vs. tumor=7).

The protein level verification of CGs in PC tissues was investigated using immunohistochemistry from the HPA (https://www.proteinatlas.org/) database (35). The PC proteome and corresponding clinical data were sourced from the CPTAC database (https://cptac-data-portal.georgetown.edu/cptacPublic), which included 90 normal and 145 tumor samples. Relative protein abundance was $\log_2$ transformed and zero centered for each gene to obtain final relative abundance values.

Establishment of cuproptosis subtypes. A total of 10 CGs [ferredoxin 1 (FDX1), DLAT, metal regulatory transcription factor 1 (MTF1), CDK inhibitor 2A (CDKN2A), glutaminase (GLS), dihydrolipoamide dehydrogenase (DLD), pyruvate dehydrogenase E1 subunit α1 (PDHA1), lipoic acid synthetase (LIAS), lipoyltransferase 1 (LIPT1) and pyruvate dehydrogenase E1 subunit β (PDHB)] were identified based on the related genes that regulate cuproptosis mentioned in a previous article (15). Consensus clustering was applied to identify distinct cuproptosis-associated patterns using the k-means algorithm in the 'ConsensusClusterPlus' package (36,37). A total of 1,000 iterations were applied to guarantee the stability of the classification. To explore the biological behaviors of CGs in PC, gene set variation analysis was performed on the Kyoto Encyclopedia of Genes and Genomes gene set (c2.cp.kegg.v7.5) from the Molecular Signatures Database (https://www.gsea-msigdb.org/gsea/msigdb/) (38).

Analysis of immune infiltration. The TME scores (including immune and stromal scores) of TCGA-PAAD tissues were estimated using several acknowledged methods, including XCELL (https://comphealth.ucsf.edu/app/xcell), TIMER (http://timer.cistrome.org/), QUANTISEQR (https://bioconductor.org/packages/quantiseqr/),MCPOUNTER (https://github.com/cit-bioinfo/mMCP-counter), EPIC (https://github.com/GfellerLab/EPIC), CIBERSORT-ABS and CIBERSORT (https://cibersortx.stanford.edu/) (39). ImmuneScore (indicating the level of immune cell infiltration), StromalScore (indicating the level of stromal cell infiltration) and ESTIMATEScore (reflecting the sum of both) for each patient were measured using the R package 'ESTIMATE' (https://bioinformatics.mdanderson.org/public-software/estimate/)). In addition, the infiltrating proportions of immune cells were assessed with the single-sample gene set enrichment analysis (ssGSEA) algorithm (https://cloud.genepattern.org) (40).

Development of the cuproptosis-associated prognostic score. The 'limma' package (https://www.plob.org/tag/limma/) (41) was used to screen the differentially expressed genes (DEGs) in the distinct CG subtypes with criteria of $|\log_2\text{-fold change}| \geq 1$ and $P<0.05$. Next, prognosis-associated genes were acquired by a univariate Cox regression analysis based on DEGs. Subsequently, the least absolute shrinkage and selection operator (LASSO) penalties were used to identify the most robust prognostic biomarkers. Finally, candidate biomarkers and their correlation coefficients were acquired to establish a

CG gene signature, defined as the risk score. The risk score was calculated as follows: Risk score=Σ (expression x corresponding coefficient).

PC cell line culture. Human PC cell lines (PATU-8988T, AsPC-1 and BxPC-3) and one normal pancreatic duct cell line (hTERT-HPNE were obtained from the China Infrastructure of Cell Line Resources, Institute of Basic Medical Sciences, Chinese Academy of Medical Sciences. The PATU-8988T, AsPC-1 and BxPC-3 cells were cultured in RPMI 1640 medium (HyClone; Cytiva), and hTERT-HPNE cells were cultured in DMEM (HyClone; Cytiva) supplemented with 100 U/ml penicillin-streptomycin (Corning, Inc.) and 10% FBS (Gibco; Thermo Fisher Scientific, Inc.) at 37˚C with 5% CO_2.

Reverse transcription-quantitative PCR (RT-qPCR). Cellular total RNA was extracted using the E.Z.N.A total RNA Kit I (Omega Bio-Tek, Inc.) and cDNA was synthesized by RT with a PrimerScript RT reagent Kit (Takara Bio, Inc.) according to the manufacturer's protocol. qPCR was performed to examine the mRNA expression levels of the FDX1, DLAT, MTF1 and CDKN2A using the SYBR Premix Ex Taq kit (Takara Bio, Inc.) with the Roche LightCycler480 PCR instrument (Roche Diagnostics). The thermocycling conditions were as follows: cDNA pre-denaturation, 95˚C for 30 sec; cDNA denaturation, 95˚C for 10 sec; and primer annealing and new strand extension, 60˚C for 30 sec. The denaturation, annealing and extension steps were repeated for a total of 40 cycles. All primers used in the present study are listed in Table I. β-actin was used as an internal control and the relative mRNA levels were calculated based on the $2^{-\Delta\Delta Cq}$ method (42).

Genomic mutation analysis and drug response prediction. To identify the differences in somatic mutations between high- and low-risk groups of patients with PC, the mutation annotation format in TCGA cohort was created with the 'maftools' R package (43). To further screen therapeutic responses to chemotherapeutics in the two groups of patients, the 'pRRophetic' package was used to evaluate the half-maximal inhibitory concentration (IC_{50}) values of chemotherapeutic drugs commonly applied to treat tumors, based on drug sensitivity data from the Genomics of Drug Sensitivity in Cancer (GDSC) dataset (https://www.cancerrxgene.org/) (44).

Additional bioinformatics and statistical analyses. The R software (version 4.4.0; R Development Core Team; https://www.r-project.org/) and its corresponding packages were applied to process, analyze and present the data. The principal component analysis (PCA) (45) was performed to assess patterns of CGs associated with cuproptosis subtypes. Data are presented as the mean ± SD from three independent experiments. Two-tailed unpaired Student's t-test or Mann-Whitney U test was applied to analyze the differences between two groups. One-way ANOVA with Tukey's post hoc test was used for differential analysis among three or more groups. Correlation was analyzed using Spearman's rank correlation coefficient. The genomic location of copy number variant (CNV) alterations in the 10 CGs across chromosomes was analyzed using the 'circlize' R package (https://github.com/jokergoo/circlize). The difference in overall survival (OS) between the two groups was estimated using the Kaplan-Meier survival curve with the R package 'survminer'(https://cran.r-project.org/web/packages/survminer/index.html) using log-rank test. Additionally, Cox regression for survival analysis was conducted using the 'survival' package (https://github.com/therneau/survival). The time-dependent receiver operating characteristic (ROC) curve was plotted using the R package 'timeROC' (https://www.rdocumentation.org/packages/timeROC/). All heatmaps were generated using 'pheatmap' package. $P<0.05$ was considered to indicate a statistically significant difference.

Results

Cuproptosis ssGSEA score is associated with improved OS in patients with PC. The flow chart of the present study is shown in Fig. S1. Regarding the intertumoral heterogeneity of cell death in patients with PC, the enrichment scores of five reported cell death modes were estimated using ssGSEA in pancreatic tumor and healthy pancreatic tissue samples from TCGA-PAAD and GTEx cohorts. The results revealed that apoptosis, necroptosis, pyroptosis and ferroptosis were aberrantly hyperactivated in tumor tissues, whereas there were no significant differences in terms of cuproptosis (Fig. 1A). Utilizing ssGSEA scores for each cell death pathway and survival data, Cox coefficient analysis was conducted for these pathways in patients with PC. Notably, among all cell death pathways, cuproptosis was the only one associated with a longer OS (Fig. 1B). These findings suggested that cuproptosis may have a key role as a positive predictive factor of improved OS in patients with PC.

Genomic mutation landscape of CGs in PC. To comprehensively elucidate the genetic landscape of CGs involved in tumorigenesis, an analysis was conducted encompassing the total somatic mutation frequency and CNVs of CGs in a cohort of 160 patients with PC sourced from TCGA dataset. Complete information of these patients is listed in Table SI. Notably, DLD, DLAT and GLS exhibited CNV amplifications, whereas PDHB and CDKN2A displayed CNV reductions (Fig. 1C). As depicted in Fig. 1D, the frequency of CDKN2A mutations was the highest, with 17% of patients harboring CDKN2A mutations, Missense and nonsense mutations were the main types of CDKN2A mutations. Fig. 1E indicates the genomic location of CNV alterations in the 10 CGs across chromosomes. The mRNA expression levels of genes are regulated by gene variants and the present findings underscored notable disparities in the genetic landscape of CGs between PC and normal samples, providing information on the potential involvement of CGs in PC tumorigenesis.

Expression and prognostic relevance of CGs in PC. Further analysis revealed that the cuproptosis score was significantly positively correlated with the expression levels of CDKN2A, followed by DLAT, suggesting that CDKN2A is the core gene involved in PC cuproptosis status; by contrast, there was no significant correlation between cuproptosis score and FDX1, MTF1, GLS, DLD, PDHA1, LIAS, LIPT1 and PDHB (Fig. 1F and G). Next, an analysis was conducted to evaluate the mRNA expression levels of CGs in PC. Compared with normal pancreatic cancer tissue from the

Table I. Primers utilized in our investigation.

Gene symbol	Primer sequence, 5'-3'
PDX1	F: GGAGCAGGATTGTGCCGTAA
	R: CTGTGGGGACGCACTAAGG
DLAT	F: GAGATGTCCCTCTAGGAACCC
	R: ACAAACACCCTTCCCTTTGGT
MTF1	F: CACAGTCCAGACAACAACATCA
	R: GCACCAGTCCGTTTTTATCCAC
CDKN2A	F: GGGTTTTCGTGGTTCACATCC
	R: CTAGACGCTGGCTCCTCAGTA
β-actin	F: CATGTACGTTGCTATCCAGGC
	R: CTCCTTAATGTCACGCACGAT

FDX1, ferredoxin 1; DLAT, dihydrolipoamide S-acetyltransferase; MTF1, metal regulatory transcription factor 1; CDKN2A, CDK inhibitor 2A; F, forward; R, reverse.

GTEx cohort, FDX1, DLAT, metal regulatory transcription factor 1 (MTF1) and CDKN2A were significantly highly expressed in PC from TCGA cohort; whereas GLS, DLD, PDHA1, LIAS, LIPT1 and PDHB were downregulated in PC (Fig. 1H). Subsequently, four genes (FDX1, DLAT, MTF1 and CDKN2A) were selected, which were highly expressed in tumor tissues, for validation in PC cell lines using RT-qPCR analysis. The results indicated that the mRNA expression levels of DLAT, MTF1 and CDKN2A exhibited substantial elevation in PC cells (PATU-8988T, AsPC-1 and BxPC-3) compared with those in the normal pancreas cell line (hTERT-HPNE). However, the expression levels of FDX1 was inconsistent among different PC cell lines; it was upregulated in PATU-8988T cells but downregulated in AsPC-1 and BxPC-3 cells compared with that in normal pancreas cells (Fig. 1I), which may be potentially attributable to the inherent heterogeneity among cell lines.

To evaluate the potential of FDX1, DLAT, MTF1 and CDKN2A as non-invasive biomarkers of risk assessment, their levels in cell-free DNA derived from blood plasma samples of patients with PC and healthy donors were analyzed. The results revealed that compared with in samples from healthy donors, the blood plasma DNA levels of DLAT was significantly increased in samples from patients with PC, whereas FDX1 was significantly decreased (Fig. 2C, G, K and O). Notably, there was no significant difference in MTF1 and CDKN2A between samples from patients with PC and healthy donors (Fig. 2K and O). Further survival analysis demonstrated that the expression of DLAT was positively associated with worse prognosis (Fig. 2H), whereas the expression of FDX1, MTF1 and CDKN2A was not related to the survival of pancreatic cancer (Fig. 2D, L and P).

Verification of protein levels of CGs was also conducted using PC proteomics analysis. The results indicated that the protein levels of FDX1 and DLAT were significantly reduced in PC tumors compared with those in normal pancreatic tissues from the GTEx project (Fig. 2A, B, E and F), while MTF1 exhibited a significant increase in PC tumors (Fig. 2I and J). No significant differences in expression were observed for CDKN2A (Fig. 2M and N). Notably, while FDX1 was shown to be increased in tumor tissues (Fig. 1H), it was decreased in in plasma samples (Fig. 2C). Although the inconsistency between the protein and transcription levels of CGs may be due to tumor heterogeneity, the present results indicated that dysregulated CG expression is involved in PC tumorigenesis.

Immunological characteristics and pathway scores of cuproptosis subtypes. Based on 'ConsensusClusterPlus', the optimal number of clusters was determined to be k=2, indicating that a division into CG cluster A (n=70) and CG cluster B (n=90) was the optimal choice for the cohort (Fig. 3A). The results of PCA also confirmed the notable intergroup distribution (Fig. 3B). Furthermore, a CGs network was constructed (Fig. 3C) to provide insights into the comprehensive genetic patterns, regulatory connections and clinical significance of CGs in patients with PC. Patients within CG cluster B exhibited worse OS compared with those in CG cluster A within TCGA cohort (log-rank test; P=0.032; Fig. 3D). The validation of clustering repeatability using the ICGC cohort is presented in Fig. S2.

The TME serves a key role in the progression of PC and has been notably associated with the limited efficacy of conventional therapeutic modalities, including chemotherapy, radiotherapy and immunotherapy (46). To comprehensively assess the TME within distinct CG subtypes, the present study quantified the immune and stromal components using the 'ESTIMATE' algorithm. Compared with CG cluster A, CG cluster B was characterized by elevated stromal score (Fig. 3E). Further analysis revealed enhanced enrichment of various immune signatures in CG cluster B, including those associated with antigen-presenting cell (APC) co-inhibition, APC co-stimulation, inflammation-promoting processes, mast cells, parainflammation, T helper 2 cells, regulatory T cells (Tregs), CAFs, TGF-β-associated extracellular matrix (ECM) and resistance to anti-programmed cell death protein (PD)-1 immunotherapy (Fig. 3F). Similarly, it was observed that the expression levels of the key immune checkpoint molecules programmed cell death ligand-1 (PD-L1) and T-cell immunoglobulin and mucin domain-containing protein 3 (TIM3) were higher within CG cluster B (Fig. 3G and H). Collectively, these findings suggested that CG cluster B may be a hallmark of stromal activation coupled with immunosuppression in PC, which offers potential options for therapeutic intervention, particularly employing PD-L1 and TIM3 inhibitors.

The results of GSEA demonstrated that CG cluster B exhibited notable enrichment in KEGG tumor-related pathways, encompassing the 'TGF-beta signaling pathway' and 'Wnt signaling pathway', as well as 'ECM receptor interaction', alongside immune-related pathways, notably 'T-cell receptor signaling pathway' and 'B-cell receptor signaling pathway' (Fig. 3I; Table SII), suggesting that alterations in these pathways affect the infiltration of immune cells in different cuproptosis subtypes.

Construction of the cuproptosis-related signature in different cohorts. In the two subclusters, a total of 224 DEGs associated with CG subtypes were identified (Table SIII). Subsequently, these DEGs were subjected to a univariate

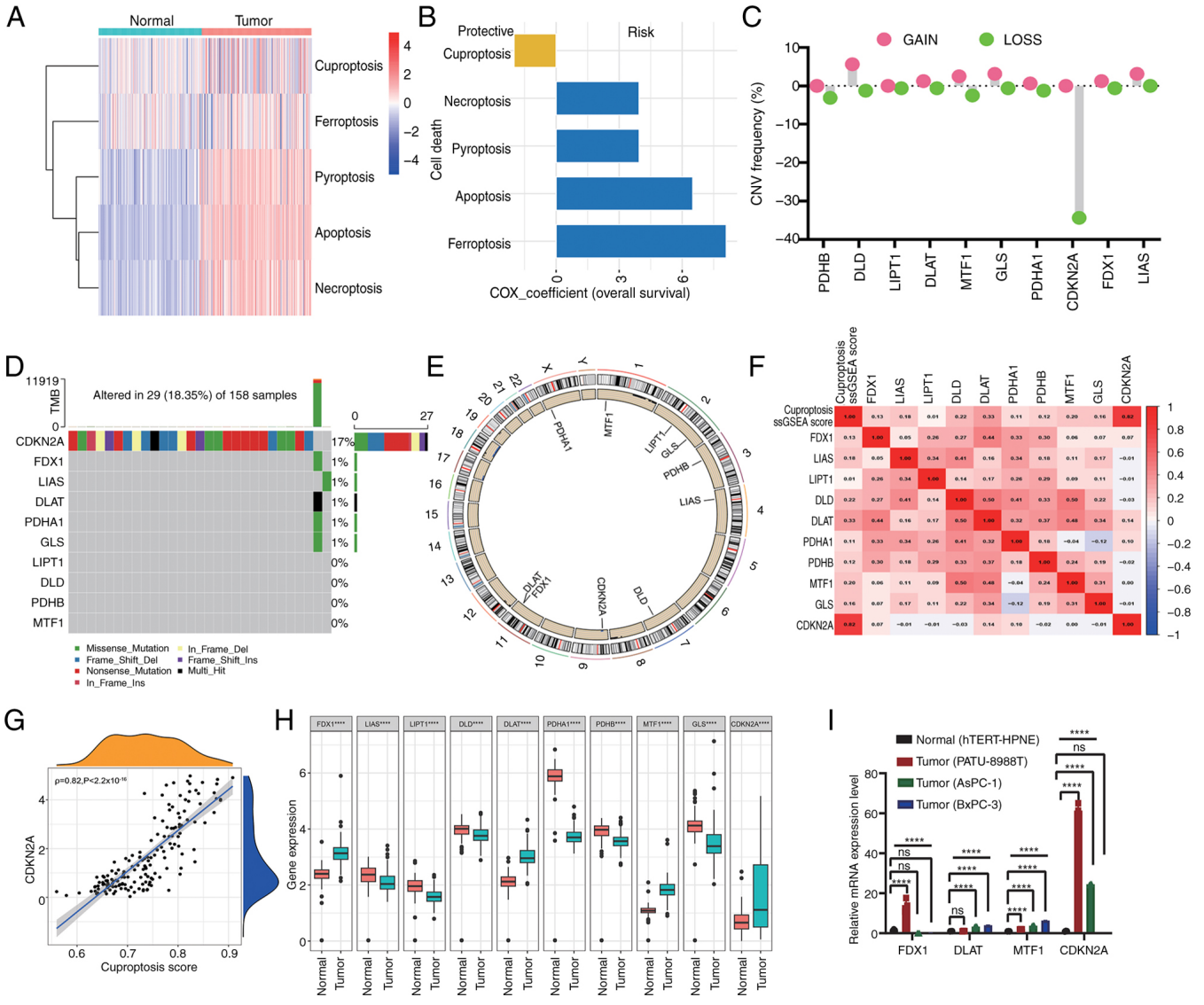


Figure 1. Genetic mutation landscape of CGs and cuproptosis subtypes in PC tumorigenesis. (A) Heatmap indicating the enrichment scores of five reported cell death pathways in pancreatic tumors and normal pancreatic samples. (B) Distribution of Cox coefficients of cell death pathways determined by univariate Cox regression analysis. (C) Frequencies of CNV gain and loss among CGs. (D) Mutation frequencies of CGs in 158 patients with PC from TCGA cohort. (E) Circular plots of chromosome distributions of CGs. (F) Heatmap displaying the correlation between cuproptosis score and mRNA expression of CGs. Red represents a positive correlation, whereas blue represents a negative correlation. (G) Correlations between the cuproptosis score and the expression of CDKN2A. (H) Expression of CGs in pancreatic tumor and healthy pancreatic samples (****P<0.0001, determined by Mann-Whitney U test). (I) Reverse transcription-quantitative PCR analyses of the mRNA expression levels of FDX1, DLAT, MTF1 and CDKN2A in PC cell lines (PATU-8988T, AsPC-1 and BxPC-3) and normal pancreatic cells (hTERT-HPNE). The results were presented as means ± SD from three times of independent experiments. A one-way ANOVA with Tukey's post hoc test was performed to analyze data. ****P<0.001. CG, cuproptosis-related gene; CNV, copy number variant; PC, pancreatic cancer; FDX1, ferredoxin 1; DLAT, dihydrolipoamide S-acetyltransferase; MTF1, metal regulatory transcription factor 1; CDKN2A, CDK inhibitor 2A; TCGA, The Cancer Genome Atlas.

Cox regression analysis, identifying 161 prognostically significant genes (P<0.05; Table SIV). To identify the most robust candidates, LASSO and multivariate Cox analyses were employed, as illustrated in Fig. 4A, along with a distribution of LASSO coefficients for the gene signature shown in Fig. 4B. Consequently, a set of five central candidates were derived, comprising three risk-associated genes [uroplakin-2 (UPK2), lactate dehydrogenase A pseudogene 7 (LDHAP7) and family member with sequence similarity 83 (FAM83A)] and two protective genes [microRNA-3677 (MIR3677) and AC068620.2], to generate a cuproptosis-related signature with the following algorithm: Risk score=(-0.426 x expression of MIR3677) + (-0.827 x expression of AC068620.2) + (0.312 x expression of UPK2) + (0.306 x expression of LDHAP7) + (0.336 x expression of FAM83A). Patients were divided into high- and low-risk score groups based on the median risk score value.

The risk score profile, as depicted in Fig. 4C and D, demonstrated a direct association between an elevated risk score, decreased OS and heightened mortality. A heatmap indicating the selected candidates is provided in Fig. S3. Kaplan-Meier analyses robustly affirmed that a high-risk score was predictive of significantly lower OS compared with a low-risk score in TCGA cohort (P<0.001; Fig. 4E) and the ICGC cohort (P<0.001; Fig. 4F). Notably, the risk score was significantly higher in deceased patients compared with

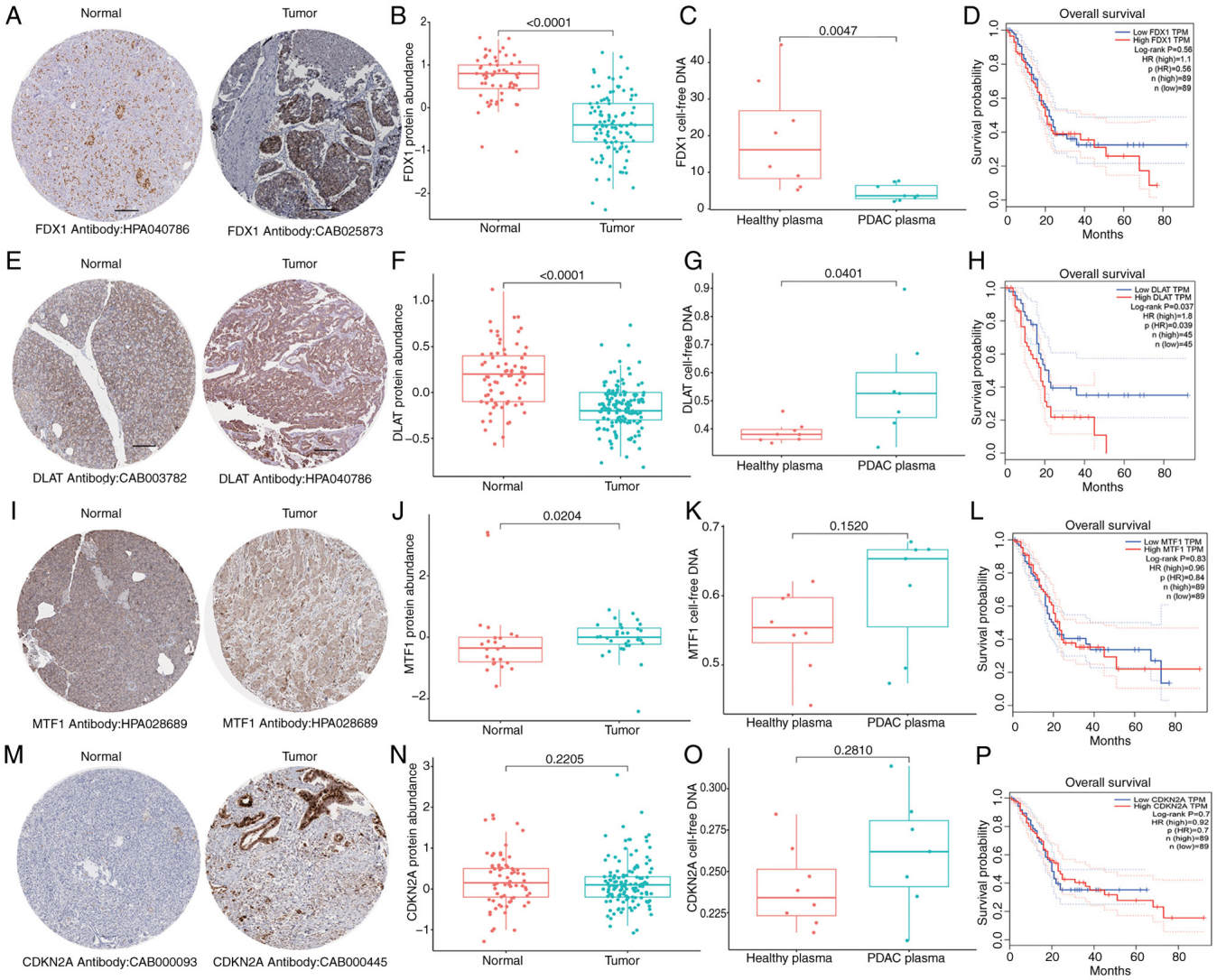


Figure 2. Expression and prognosis of cuproptosis-related genes in PC. Histological expression levels of (A) FDX1, (E) DLAT, (I) MTF1 and (M) CDKN2A from the Human Protein Atlas database; the antibody type used in immunohistochemistry and the patient ID of tissue specimens are shown at the bottom of each image. Different protein levels of (B) FDX1, (F) DLAT, (J) MTF1 and (N) CDKN2A in pancreatic tumor and healthy pancreas samples from the Clinical Proteomic Tumor Analysis Consortium database (the Mann-Whitney U test was performed to analyze data). Different cell-free DNA levels of (C) FDX1, (G) DLAT, (K) MTF1 and (O) CDKN2A in blood plasma samples of normal healthy donors and pancreatic cancer from the GEO database (the Mann-Whitney U test was performed to analyze data). (D, H, L and P) Survival analysis of (D) FDX1, (H) DLA, (L) MTF1 and (P) CDKN2A in The Cancer Genome Atlas-pancreatic adenocarcinoma cohort. FDX1, ferredoxin 1; DLAT, dihydrolipoamide S-acetyltransferase; MTF1, metal regulatory transcription factor 1; CDKN2A, CDK inhibitor 2A; PC, pancreatic cancer.

those patients who were alive at the time of follow-up in both TCGA and ICGC cohorts (Fig. 4G and H). Fig. 4I displayed the distribution of patients in the two CG clusters and two risk score groups. Furthermore, Fig. 4J illustrated the patient distribution across the two CG clusters and two risk score groups. Notably, patients within CG cluster A displayed a lower risk score, whereas those in CG cluster B exhibited a higher risk score. The present study then explored the correlation between MIR3677, AC068620.2, UPK2, LDHAP7 and FAM83A in the prognostic gene signature and the enrichment of tumorigenesis-associated pathways; it was concluded that the majority of tumorigenesis-associated pathways, such as the 'TGF-β signaling pathway', 'Wnt signaling pathway' and 'TP53 signaling pathway', were closely associated with the expression of MIR3677, AC068620.2, LDHAP7 and FAM83A) (Fig. 4K).

Prognostic potential of the cuproptosis-related signature in different cohorts. Subsequently, nomograms were developed to predict patient outcomes across different datasets, due to the notable association between risk score and prognosis. The results demonstrated that risk score functioned as an independent prognostic factor for OS, even when accounting for clinical variables, in patients with PC from both TCGA and ICGC cohorts (Fig. 5A and D). Furthermore, the predictive accuracy of the risk score for 1-, 2- and 3-year survival rates was quantified by calculating the area under the curve (AUC) in TCGA cohort (0.732, 0.764 and 0.785, respectively) and the ICGC cohort (0.939, 0.914 and 0.890, respectively) (Fig. 5B and E). To assess the predictive precision of risk score compared with clinical variables for patients with PC, the AUC values for these factors were calculated (Fig. 5C and F). Notably, risk score

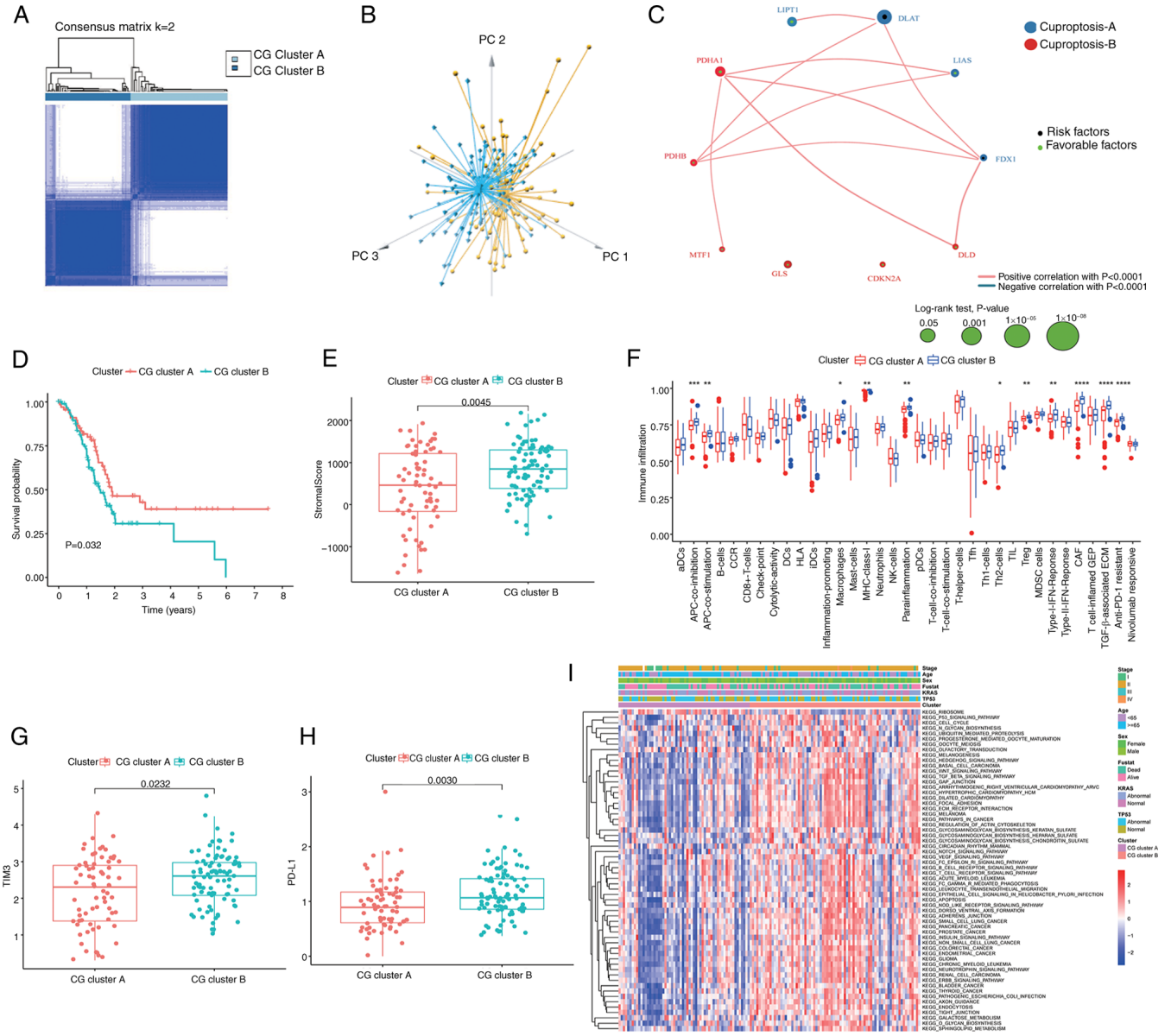


Figure 3. Immunological characteristics and pathway scores of cuproptosis subtypes. (A) Consensus matrix heatmap defining two clusters (k=2) and their correlation area. (B) Principal component analysis demonstrating two distinct subtypes of cuproptosis in TCGA cohort. (C) A network of correlations including CGs in TCGA-pancreatic adenocarcinoma cohort. (D) Kaplan-Meier plot of overall survival of patients with PC split according to CG clusters, analyzed by log-rank test. (E) Association between the two cuproptosis subtypes and stromal score in PC. (F) Abundance of the infiltration of 35 tumor microenvironment cells of patients with PC split according to two cuproptosis subtypes. Expression levels of (G) TIM3 and (H) PD-L1 in the patients with PC split according to two cuproptosis subtypes. (I) Gene Set Variation Analysis of the biological pathways of two cuproptosis subtypes in PC samples from TCGA and International Cancer Genome Consortium cohorts. ****P<0.0001, ***P<0.001, **P<0.01, *P<0.05, not significant (P>0.05), analyzed using the Mann-Whitney U test. CG, cuproptosis-related gene; PC, pancreatic cancer; TCGA, The Cancer Genome Atlas; TIM3, T-cell immunoglobulin and mucin domain-containing protein 3; PD-L1, programmed cell death ligand-1.

consistently exhibited robust AUC values comparable with other clinical variables, underscoring its performance in prognostic assessment for patients with PC. Furthermore, nomograms were constructed incorporating risk score and various clinical features tailored to individual patients with PC (Fig. 5G and H). The results demonstrated that risk score had notable predictive performance.

Association of immune status and immunotherapy with the cuproptosis-related signature in PC. The present findings suggested a substantial association between CG subtypes and stromal accumulation in PC. Consequently, a comprehensive analysis of the immune interactions within both high- and low-risk score groups was conducted. A high-risk score exhibited an inverse relationship with key immune cell populations, including CD8 and CD4 T cells, B cells, monocytes and natural killer cells, while demonstrating positive associations with M0 macrophages, M1 macrophages, neutrophils and CAFs (Fig. 6A; Table SV). These observations suggested an intricate immune microenvironment characterized by stromal activation and immunosuppression in the high-risk score group. Furthermore, the expression profiles of immune checkpoint proteins (ICPs) were examined. Within the high-risk score group, significant upregulation of certain ICPs

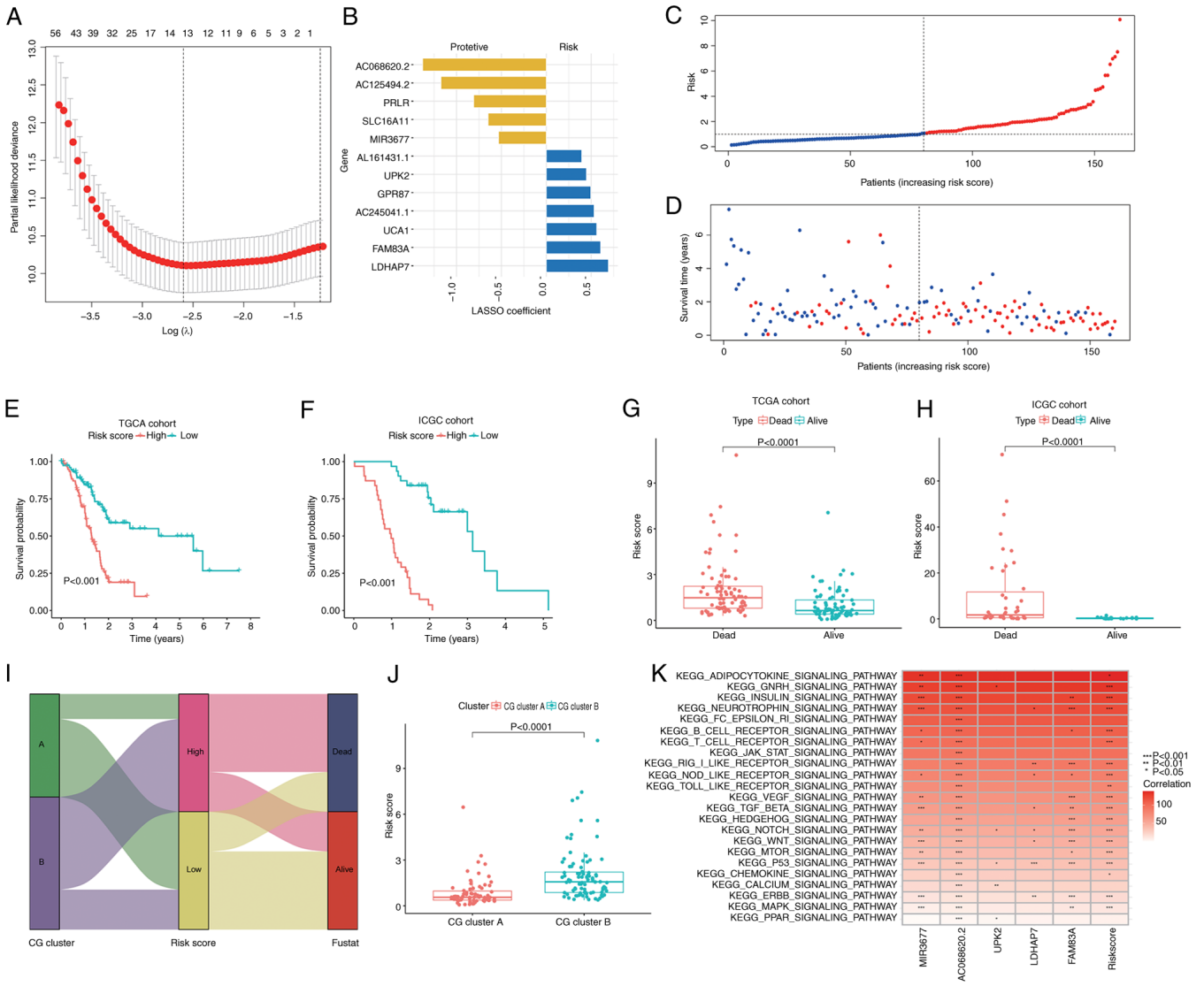


Figure 4. Construction and validation of the cuproptosis-related signature in different cohorts. (A) LASSO Cox regression model was applied to identify the most robust biomarkers. (B) Distribution of LASSO coefficients of the CG signature. (C) Ranked dot plot demonstrating the risk score distribution and patient survival status. (D) Scatter plot demonstrating the patient survival status. (E and F) Kaplan-Meier curves were used to analyze the survival of patients with PC with high- and low-risk scores in TCGA and ICGC cohorts. (G and H) Differences in risk score between dead and alive patients with PC. (I) Alluvial diagram of cuproptosis subtype distributions in groups with different risk scores, molecular subtypes and survival outcomes. (J) Differences in risk score between CG clusters and gene subtypes (data were analyzed using the Mann-Whitney U test). (K) Association analysis between tumorigenesis-associated pathways and the selected genes. LASSO, least absolute shrinkage and selection operator; CG, cuproptosis-related gene; PC, pancreatic cancer; TCGA, The Cancer Genome Atlas; ICGC, International Cancer Genome Consortium; PC, pancreatic cancer; MIR3677, microRNA-3677; UPK2, uroplakin-2; LDHAP7, lactate dehydrogenase A pseudogene 7; FAM83A, family member with sequence similarity 83.

was observed, including CD70, CD44, CD276 and VTCN1, while others such as CD200, TNFRSF4, CD160, ADORA2A and TNFRSF14 exhibited significant downregulation (Fig. 6B). These findings hold promise in offering potential immunotherapeutic options for the clinical management of patients with PC.

Considering the well-established association between stromal activation and tumor immune evasion (47-49), the present investigation was extended to delineate distinct gene signatures among patients with different risk scores. Among patients with a high-risk score, heightened expression of stromal activation-associated signatures, such as CAFs and the TGF-β-associated ECM, was observed (Fig. 6C and D). The expression of a signature associated with resistance to anti-PD-1 therapy was also more pronounced in patients with a high-risk score (Fig. 6E), suggesting a potential challenge in achieving favorable responses to anti-PD-1 immunotherapy within this subgroup. In addition, risk score was compared with currently known biomarkers [such as PD-L1, microsatellite instability score and tumor mutational burden (TMB)] to evaluate the efficacy of immunotherapy and the results revealed that the risk score had enhanced potential to predict prognosis (Fig. 6F), despite the higher correlation between PD-L1 and resistance to anti-PD-1 score (Fig. 6G). The aforementioned results suggested that the risk score may be closely associated with tumor immunotherapeutic markers and has the potential to be used as a novel immunotherapeutic marker.

Genomic mutation analysis for the cuproptosis-related signature. Prior research has consistently demonstrated

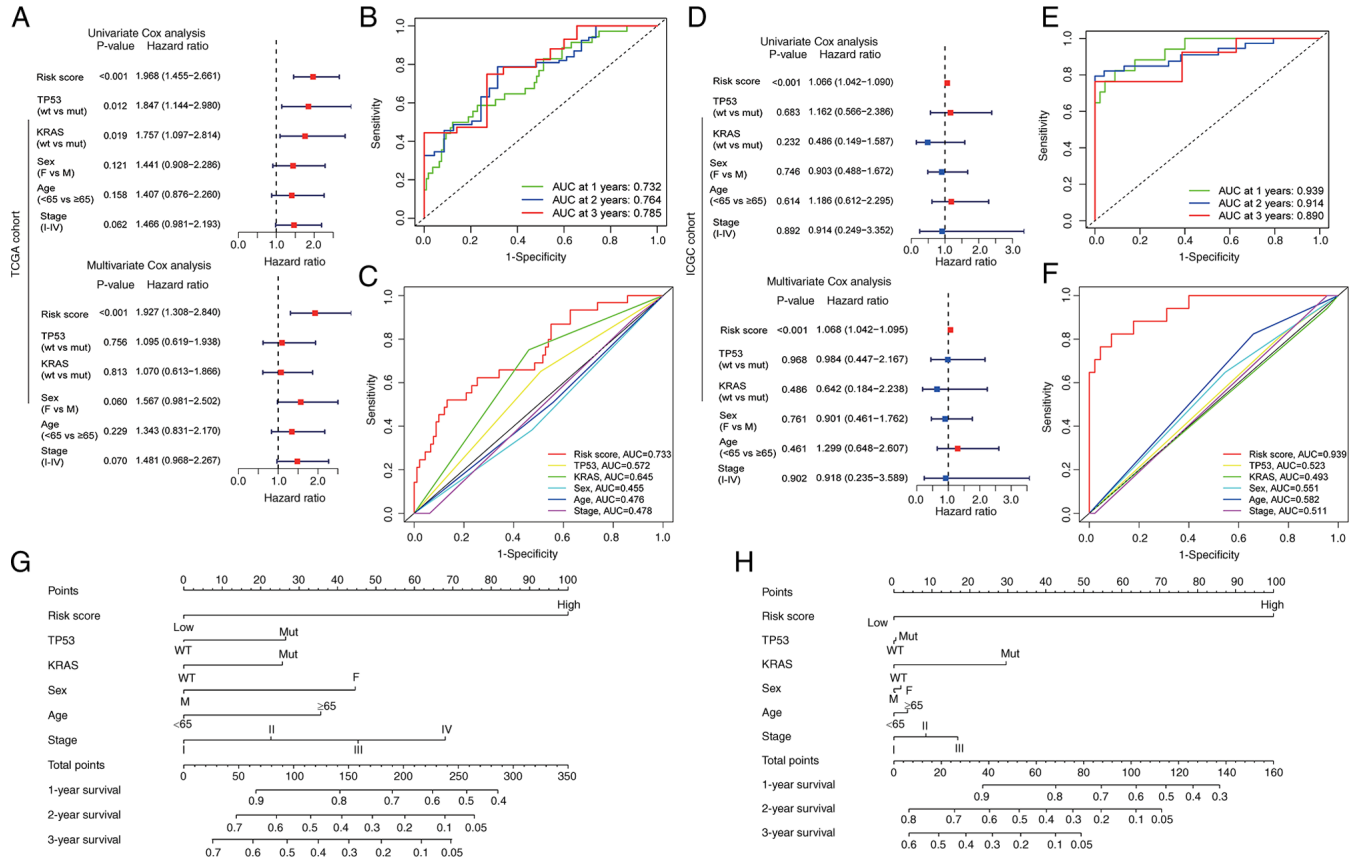


Figure 5. Prognostic potential of the cuproptosis-related signature in different cohorts. (A and D) Univariate and multivariate Cox regression analyses demonstrated that risk score was an independent risk factor for OS in the (A) training cohort and (D) validation cohort. (B) ROC curve to predict the sensitivity and specificity of 1-, 2- and 3-year survival according to the risk score in TCGA cohort. (E) ROC curve to predict the sensitivity and specificity of 1-, 2- and 3-year survival according to the risk score in ICGC cohort. (C) Time-dependent ROC curve depicting the predictive precision of risk score and clinical features in TCGA cohort. (F) Time-dependent ROC curve depicting the predictive precision of risk score and clinical features in ICGC cohort. (G) Nomogram to predict the 1-, 2- and 3-year OS of patients with pancreatic cancer in TCGA cohort. (H) Nomogram to predict the 1-, 2- and 3-year OS of patients with pancreatic cancer in ICGC cohort. ICGC, International Cancer Genome Consortium; OS, overall survival; ROC, receiver operating characteristic; TCGA, The Cancer Genome Atlas; AUC, area under the curve; wt, wild-type; mut, mutant; M, male; F, female.

an association between TMB and immune infiltration, as well as its prognostic implications across various types of cancer (50-52). In the present comprehensive mutation dataset analysis, a significantly elevated TMB score was observed in the high-risk score group when compared with the low-risk score group (Fig. 6H). Furthermore, survival analysis revealed a markedly improved prognosis among patients with lower TMB scores and lower risk scores compared with higher TMB scores and higher risk scores (P<0.001; Fig. 6I). PC is characterized by a complex genetic landscape, with frequent somatic mutations occurring in key driver genes, notably KRAS, CDKN2A, TP53 and SMAD4 (53). In this context, an in-depth assessment of the distribution patterns of somatic alterations between the two distinct risk score groups within TCGA-PAAD cohort was conducted. Notably, TP53, KRAS, CDKN2 and SMAD4 emerged as the primary mutated genes in both high- and low-risk score groups (Fig. 6J and K). Patients classified in the high-risk score category exhibited substantially higher frequencies of TP53, KRAS, CDKN2 and SMAD4 mutations compared with their counterparts in the low-risk score group. Conversely, the mutation percentages for TTN, RNF43, MUC16 and RYR1 were not significantly different between the groups. These findings underscore the complex interplay between TMB, risk score and the genetic landscape of PC, shedding light on potential prognostic markers and therapeutic options.

Association of the cuproptosis-related signature with cancer stem cell (CSC) score and clinical outcomes in PC. CSCs promote tumorigenesis and metastasis in PC (54,55). PC stem cell proliferation is notably inhibited by diethyldithiocarbamate-copper complex loaded into hyaluronic acid-decorated liposomes (56). Therefore, the present study analyzed the correlation between the cuproptosis-related signature and CSC index values and a weak correlation was observed between the risk score and the CSC index (ρ=0.23, P=0.0057; Fig. 7A). There was a higher CSC score in the high-risk score group compared with that in the low-risk score group (P=0.0024; Fig. 7B), which indicates that stem cells have more notable stemness and lower differentiation characteristics in the high-risk score group. Furthermore, to investigate the impact of risk score on clinical outcomes in patients with PC, therapeutic information and clinical outcomes from TCGA were assessed. As shown in Fig. 7C and D, a high-risk score was associated with a higher rate of progressive disease and stable disease.

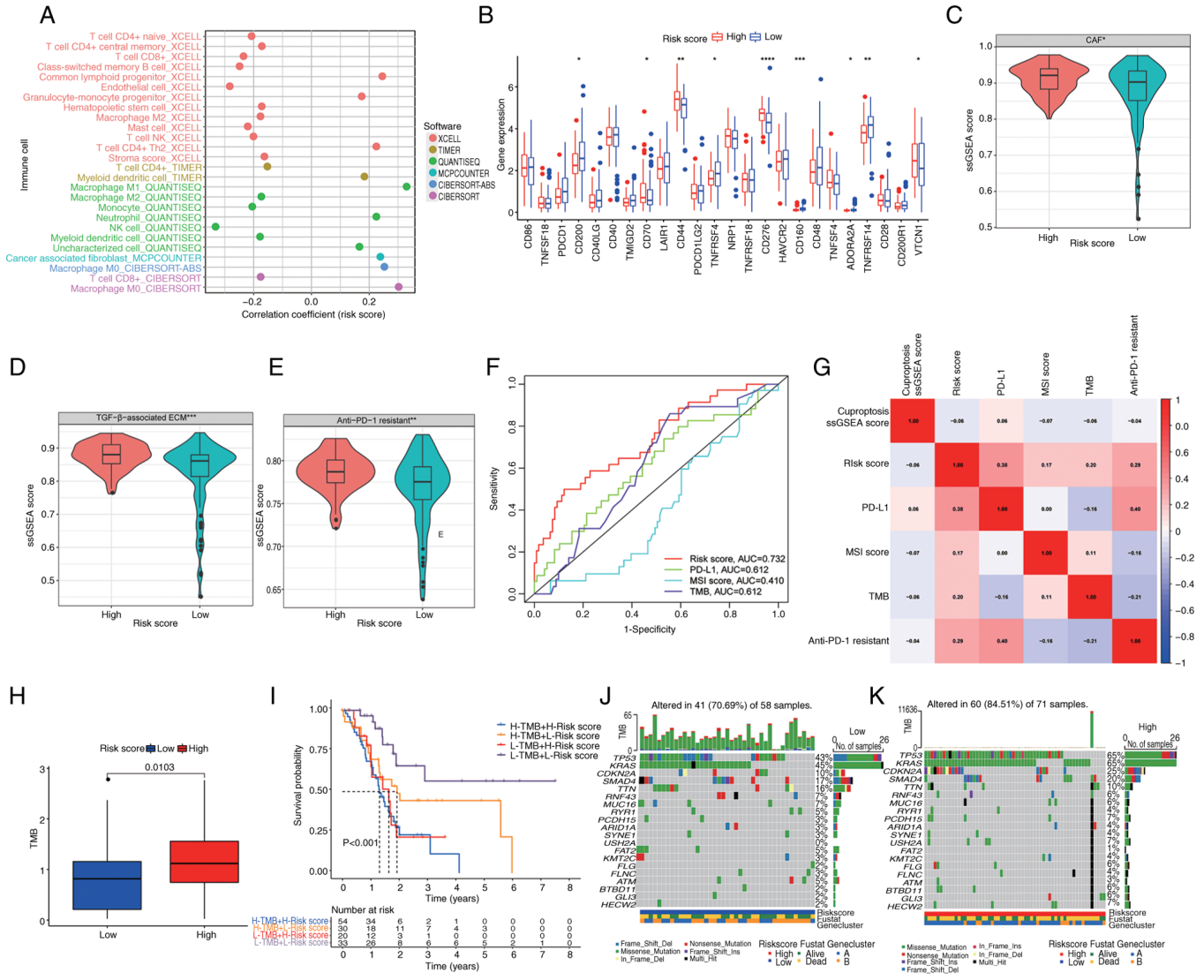


Figure 6. Association of immune status and immunotherapy with the cuproptosis-related signature in pancreatic cancer. (A) Correlation of immune infiltration with risk score. (B) Boxplots of immune checkpoint gene expression in distinct risk score groups. Boxplots indicating ssGSEA score of (C) CAFs, (D) TGF-β-associated ECM and (E) anti-PD-1 immunotherapy response in different risk score groups. (F) Time-dependent receiver operating characteristic curves depicting the predictive precision of risk score and existing biomarkers (PD-L1, MSI score and TMB) for evaluating the efficacy of immunotherapy. (G) Correlation analysis between risk score, cuproptosis ssGSEA score, PD-L1, MSI score, TMB and anti-PD-1 immunotherapy response. (H) TMB in different risk score groups. (I) Survival analysis among four patient groups stratified by both TMB and risk score. (J and K) Waterfall plot of somatic mutation features established with low and high-risk scores. Each column represents an individual patient. The upper bar plot indicates TMB, the number on the right indicates the mutation frequency in each gene. The right bar plot demonstrates the proportion of each variant type. ****P<0.0001, ***P<0.001, **P<0.01, *P<0.05, analyzed using the Mann-Whitney U test. MSI, microsatellite instability; TMB, tumor mutational burden; ssGSEA, single-sample gene set enrichment analysis; CAFs, cancer-associated fibroblasts; ECM, extracellular matrix; PD-1, programmed cell death protein-1; PD-L1, programmed cell death ligand-1; AUC, area under the curve.

Drug susceptibility according to the cuproptosis-related signature. Subsequently, to confirm the efficacy of risk score as a predictive biomarker for therapeutic response in patients with PC, the IC_{50} values of 138 chemotherapeutic drugs from the GDSC dataset were assessed in TCGA-PAAD dataset. A total of 29 drugs were more sensitive in patients with a low-risk score (P<0.05; Table SVI), among which the leading chemotherapeutic agents were: ABT-888, nutlin-3a, nilotinib and EHT 1864 (Fig. 7E-H). A total of 54 drugs demonstrated an improved response in patients with a high-risk score (P<0.05; Table SVII), among which the top four chemotherapeutic drugs were Z-LLNle-CHO, RDEA119, A-443654 and A-770041 (Fig. 7I-L). Together, these findings indicated that risk score may be associated with drug sensitivity.

Discussion

For patients with advanced PC, conventional treatments including chemotherapy and targeted therapy have little effect on improving prognoses and limiting tumor progression (3,7,23,47,49). It is therefore urgent to screen valuable biomarkers that can classify patients with different molecular characteristics into diverse subgroups, and predict prognosis and treatment. Copper accumulation triggers mitochondrial-driven cell death, known as cuproptosis, which is

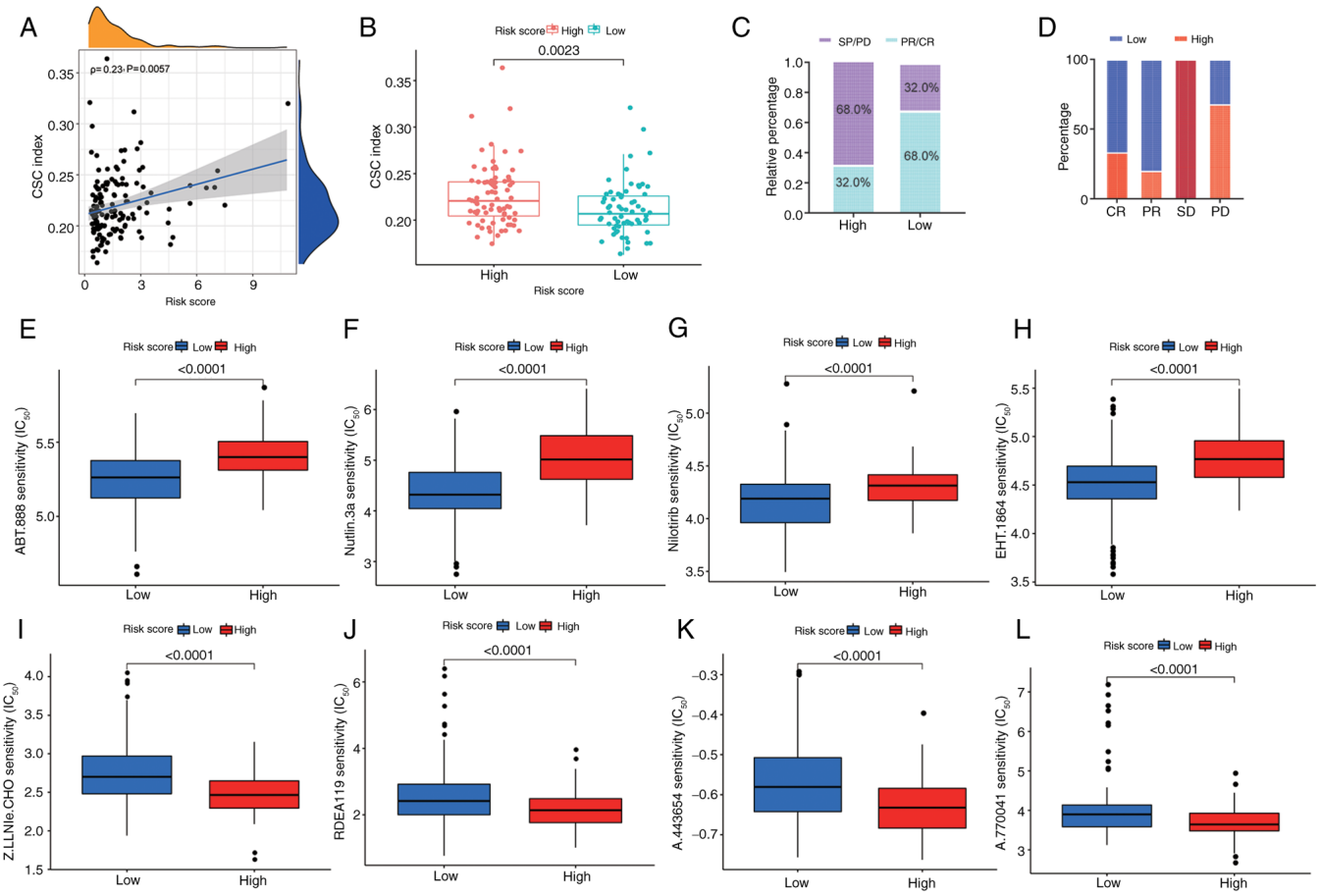


Figure 7. Associations between cuproptosis-related signature and CSC score, clinical outcomes and drug susceptibility in PC. (A) Spearman's rank correlation analysis of risk score and CSC index. (B) CSC score in distinct risk score groups. (C) Ratio of worse outcomes after surgery was notably elevated in the higher risk score group. (D) Proportion of clinical outcomes in patients with PC with high- and low-risk scores after surgery. Top four chemotherapeutic drugs, (E) ABT-888, (F) nutlin-3a, (G) nilotinib and (H) EHT 1864 exhibiting sensitivity for patients with PC with a low-risk score. Top four chemotherapeutic drugs (I) Z-LLNle-CHO, (J) RDEA119, (K) A-443654 and (L) A-770041 exhibiting sensitivity for patients with PC with a high-risk score. Data were analyzed using the Mann-Whitney U test. CSC, cancer stem cell; PC, pancreatic cancer; SD, stable disease; PD, progressive disease; CR, complete response; PR, partial response; IC_{50}, half maximal inhibitory concentration.

associated with tumor progression (20,21,32,57). Hence, exploring the regulatory effects of cuproptosis on tumors and its molecular mechanisms is key, as it may provide novel directions and strategies for clinical cancer treatment.

The present study indicated that apoptosis, necroptosis, pyroptosis and ferroptosis were aberrantly hyperactivated in PC tissues and cuproptosis exhibited the only protective effect on survival compared with the other cell death modes. The present study further analyzed the gene variants of CGs. Among 10 CGs, the frequency of CDKN2A mutations was the highest. Correlation analysis revealed that CDKN2A and DLAT were associated with cuproptosis score. The aggregation of gene mutations leads to tumorigenesis and gene mutations in PC, which may notably impact immunotherapy response. It has been reported that mutations in CDKN2A are frequently identified in a number of primary tumors and patients with melanoma carrying CDKN2A gene mutations respond better to immunotherapy (50). The latest research has indicated that copper nanoparticles enhance cuproptosis and immunotherapy response in PC (58). This evidence suggests that CDKN2A mutations may be associated with cuproptosis and could affect immunotherapy. The present study further verified the protein level of CGs using PC proteomics analysis and the results indicated an inconsistency between the protein and transcription levels of CGs, which may be associated with the heterogeneity in human tissue and plasma samples.

Previous studies have shown that the combination of Tussah silk fibroin nanoparticles and PD-L1 effectively induces cuproptosis and reshapes the TME in PC (59,60). In addition, advanced cancer-infiltrating and killing abilities of natural killer, $CD8^+$ T cells and neutrophils have been reported to be associated with FDX1 expression; the levels of FDX1 are decreased in several types of cancer and reflect the level of immune cell infiltration (61). Targeted activation of cuproptosis pathways may favor re-activation of the TME towards the eradication of cancer cells (57). Targeted activation of CGs may be investigated as priming or contributing factors for improving current immune checkpoint inhibitor (ICI) immunotherapy (20,24).

PC is characterized by extensive stromal involvement, which makes classifying precise tumor-specific molecular subtypes difficult (47). Stromal cells, as a vital component of the TME, serve an important role in monitoring tumor immune evasion, even in the presence of abundant immune cells. Increasing evidence has also shown the effects of stromal cells on tumor

progression and therapeutic resistance (30,46). Consistently, the present study revealed that the patients with PC in CG cluster B had a worse OS and a higher stromal score, as well as increased enrichment of Tregs, CAFs, TGF-β-associated ECM and anti-PD-1 resistance, thus limiting antitumor immunity and leading to poor survival. Previous studies have demonstrated that CAFs can attract Tregs and enhance the capacity of inhibiting effector T-cell proliferation (62,63). In addition, TGF-β-associated ECM has been shown to be associated with CAFs, immune evasion and immunotherapy failure (48,64). Furthermore, stromal activation signatures, such as CAFs and TGF-β-associated ECM, were highly expressed in patients with a high-risk score. Notably, a higher anti-PD-1 resistant-related signature was also observed in the high-risk score group, confirming the existing conclusions. Thus, based on the aforementioned results, one possible mechanism for CGs in the PC TME was suggested: CGs could stimulate extensive stromal involvement of tumors and regulate CAF activation, as well as TGF-β-associated ECM hyperactivation, which in turn may recruit immunosuppressive cell populations, such as Tregs, causing tumor immune escape.

In addition, a CG signature was established to predict clinical outcome, immunotherapy response and chemotherapy susceptibility in PC. By integrating the risk score and clinical variables, a quantitative nomogram was generated to further improve the performance and facilitate the clinical utility of the signature. To determine potential drug therapy targets for patients with PC, the present study identified the potential sensitive drugs for patients in diverse risk score groups. The results indicated that the risk score may be a robust prognostic biomarker, which could contribute to precise risk stratifications and offer clues for combining customized prognostic prediction with individualized therapy. For patients with a high-risk score, the present study identified the latent therapeutic drugs that could effectively improve their survival. For patients with a low-risk score, clinicians may consider adopting ICI immunotherapy to improve the survival of patients with PC.

In conclusion, these findings highlighted the overall phenotypic role of CGs in PC and identified obvious differences in prognosis, clinical features and TME characteristics between two CG subtypes. Furthermore, a novel prognostic CG signature was defined in PC; this CG score may act as a robust prognostic indicator for patients with PC, which offers potential for precise risk stratification and predictive markers for effective immunotherapy strategies.

However, certain limitations of the present study should be acknowledged. First, the present study did not include any datasets associated with immunotherapy for PC and could not be verified, therefore future research is warranted for the validation in PC immunotherapy datasets. Second, the CG scoring system is a gene set consisting of five genes, thus, it cannot be quantified in *in vivo* and *in vitro* experiments. The utility of the CG scoring system is limited to retrospective studies of tumor tissue specimens; therefore, future studies can evaluate and select the most valuable genes for experimental verification.

Acknowledgements

Not applicable.

Funding

The present study was funded by the National Natural Science Foundation of China (grant no. 82403378), the China National Postdoctoral Program for Innovative Talents (grant no. BX20240072) and the China Postdoctoral Science Foundation (grant no. 2024M750525).

Availability of data and materials

The data generated in the present study may be requested from the corresponding author.

Authors' contributions

WG conceptualized and designed the present study, prepared the materials, collected data, performed the data analysis and wrote first draft of the manuscript. YoW and DS prepared the materials, collected data and revised the manuscript. MY and YaW cultivated pancreatic cancer cell lines, prepared the total cellular RNA samples and reviewed the manuscript. WG, YoW, DS, MY and YaW confirm the authenticity of the data in the present study. All authors read and approved the final manuscript.

Ethics approval and consent to participate

Not applicable.

Patient consent for publication

Not applicable.

Competing interests

The authors declare that they have no competing interests.

References

1. Siegel RL, Giaquinto AN and Jemal A: Cancer statistics, 2024. CA Cancer J Clin 74: 12-49, 2024.
2. Stoop TF, Javed AA, Oba A, Koerkamp BG, Seufferlein T, Wilmink JW and Besselink MG: Pancreatic cancer. Lancet 405: 1182-1202, 2025.
3. Cai J, Chen H, Lu M, Zhang Y, Lu B, You L, Zhang T, Dai M and Zhao Y: Advances in the epidemiology of pancreatic cancer: Trends, risk factors, screening, and prognosis. Cancer Lett 520: 1-11, 2021.
4. Bergman PJ: Cancer immunotherapy. Vet Clin North Am Small Anim Pract 54: 441-468, 2024.
5. Yang K, Halima A and Chan TA: Antigen presentation in cancer-mechanisms and clinical implications for immunotherapy. Nat Rev Clin Oncol 20: 604-623, 2023.
6. Bednar F and Pasca di Magliano M: Context-dependent immune responses explain pancreatic cancer immunoresistance. Cancer Cell 37: 261-263, 2020.
7. Farhangnia P, Khorramdelazad H, Nickho H and Delbandi AA: Current and future immunotherapeutic approaches in pancreatic cancer treatment. J Hematol Oncol 17: 40, 2024.
8. Fan JQ, Wang MF, Chen HL, Shang D, Das JK and Song J: Current advances and outlooks in immunotherapy for pancreatic ductal adenocarcinoma. Mol Cancer 19: 32, 2020.
9. Gibellini L and Moro L: Programmed cell death in health and disease. Cells 10: 1765, 2021.
10. Tong X, Tang R, Xiao M, Xu J, Wang W, Zhang B, Liu J, Yu X and Shi S: Targeting cell death pathways for cancer therapy: Recent developments in necroptosis, pyroptosis, ferroptosis, and cuproptosis research. J Hematol Oncol 15: 174, 2022.

11. Liu Y, Fleishman JS, Wang H and Huo L: Pharmacologically targeting ferroptosis and cuproptosis in neuroblastoma. Mol Neurobiol 62: 3863-3876, 2025.
12. Tsang T, Davis CI and Brady DC: Copper biology. Curr Biol 31: R421-R427, 2021.
13. Chen L, Min J and Wang F: Copper homeostasis and cuproptosis in health and disease. Signal Transduct Target Ther 7: 378, 2022.
14. Kahlson MA and Dixon SJ: Copper-induced cell death. Science 375: 1231-1232, 2022.
15. Tsvetkov P, Coy S, Petrova B, Dreishpoon M, Verma A, Abdusamad M, Rossen J, Joesch-Cohen L, Humeidi R, Spangler RD, *et al*: Copper induces cell death by targeting lipoylated TCA cycle proteins. Science 375: 1254-1261, 2022.
16. Tang D, Chen X and Kroemer G: Cuproptosis: A copper-triggered modality of mitochondrial cell death. Cell Res 32: 417-418, 2022.
17. Sun L, Zhang Y, Yang B, Sun S, Zhang P, Luo Z, Feng T, Cui Z, Zhu T, Li Y, *et al*: Lactylation of METTL16 promotes cuproptosis via m^{6}A-modification on FDX1 mRNA in gastric cancer. Nat Commun 14: 6523, 2023.
18. Jiang Y, Huo Z, Qi X, Zuo T and Wu Z: Copper-induced tumor cell death mechanisms and antitumor theragnostic applications of copper complexes. Nanomedicine (Lond) 17: 303-324, 2022.
19. Tang D, Kroemer G and Kang R: Targeting cuproplasia and cuproptosis in cancer. Nat Rev Clin Oncol 21: 370-388, 2024.
20. Liu WQ, Lin WR, Yan L, Xu WH and Yang J: Copper homeostasis and cuproptosis in cancer immunity and therapy. Immunol Rev 321: 211-227, 2024.
21. Xie J, Yang Y, Gao Y and He J: Cuproptosis: Mechanisms and links with cancers. Mol Cancer 22: 46, 2023.
22. Tarin M, Babaie M, Eshghi H, Matin MM and Saljooghi AS: Elesclomol, a copper-transporting therapeutic agent targeting mitochondria: From discovery to its novel applications. J Transl Med 21: 745, 2023.
23. O'Day S, Gonzalez R, Lawson D, Weber R, Hutchins L, Anderson C, Haddad J, Kong S, Williams A and Jacobson E: Phase II, randomized, controlled, double-blinded trial of weekly elesclomol plus paclitaxel versus paclitaxel alone for stage IV metastatic melanoma. J Clin Oncol 27: 5452-5458, 2009.
24. Qin Y, Liu Y, Xiang X, Long X, Chen Z, Huang X, Yang J and Li W: Cuproptosis correlates with immunosuppressive tumor microenvironment based on pan-cancer multiomics and single-cell sequencing analysis. Mol Cancer 22: 59, 2023.
25. Gadiyar V, Lahey KC, Calianese D, Devoe C, Mehta D, Bono K, Desind S, Davra V and Birge RB: Cell death in the tumor microenvironment: Implications for cancer immunotherapy. Cells 9: 2207, 2020.
26. Gao L, Shay C and Teng Y: Cell death shapes cancer immunity: Spotlighting PANoptosis. J Exp Clin Cancer Res 43: 168, 2024.
27. Hänggi K and Ruffell B: Cell death, therapeutics, and the immune response in cancer. Trends Cancer 9: 381-396, 2023.
28. Zhou Q, Meng Y, Li D, Yao L, Le J, Liu Y, Sun Y, Zeng F, Chen X and Deng G: Ferroptosis in cancer: From molecular mechanisms to therapeutic strategies. Signal Transduct Target Ther 9: 55, 2024.
29. Du T, Gao J, Li P, Wang Y, Qi Q, Liu X, Li J, Wang C and Du L: Pyroptosis, metabolism, and tumor immune microenvironment. Clin Transl Med 11: e492, 2021.
30. Han X, Zhang WH, Wang WQ, Yu XJ and Liu L: Cancer-associated fibroblasts in therapeutic resistance of pancreatic cancer: Present situation, predicaments, and perspectives. Biochim Biophys Acta Rev Cancer 1874: 188444, 2020.
31. Storrs EP, Chati P, Usmani A, Sloan I, Krasnick BA, Babbra R, Harris PK, Sachs CM, Qaium F, Chatterjee D, *et al*: High-dimensional deconstruction of pancreatic cancer identifies tumor microenvironmental and developmental stemness features that predict survival. NPJ Precis Oncol 7: 105, 2023.
32. Wang W, Lu K, Jiang X, Wei Q, Zhu L, Wang X, Jin H and Feng L: Ferroptosis inducers enhanced cuproptosis induced by copper ionophores in primary liver cancer. J Exp Clin Cancer Res 42: 142, 2023.
33. Reggiardo RE, Maroli SV, Peddu V, Davidson AE, Hill A, LaMontagne E, Aaraj YA, Jain M, Chan SY and Kim DH: Profiling of repetitive RNA sequences in the blood plasma of patients with cancer. Nat Biomed Eng 7: 1627-1635, 2023.
34. Song CX, Yin S, Ma L, Wheeler A, Chen Y, Zhang Y, Liu B, Xiong J, Zhang W, Hu J, *et al*: 5-Hydroxymethylcytosine signatures in cell-free DNA provide information about tumor types and stages. Cell Res 27: 1231-1242, 2017.
35. Digre A and Lindskog C: The human protein atlas-spatial localization of the human proteome in health and disease. Protein Sci 30: 218-233, 2021.
36. Sabah A, Tiun S, Sani NS, Ayob M and Taha AY: Enhancing web search result clustering model based on multiview multirepresentation consensus cluster ensemble (mmcc) approach. PLoS One 16: e0245264, 2021.
37. Seiler M, Huang CC, Szalma S and Bhanot G: ConsensusCluster: A software tool for unsupervised cluster discovery in numerical data. OMICS 14: 109-113, 2010.
38. Hänzelmann S, Castelo R and Guinney J: GSVA: Gene set variation analysis for microarray and RNA-seq data. BMC 14: 7, 2013.
39. Wu D, Liu Y, Liu J, Ma L and Tong X: Myeloid cell differentiation-related gene signature for predicting clinical outcome, immune microenvironment, and treatment response in lung adenocarcinoma. Sci Rep 14: 17460, 2024.
40. Huang L, Wu C, Xu D, Cui Y and Tang J: Screening of important factors in the early sepsis stage based on the evaluation of ssGSEA algorithm and ceRNA regulatory network. Evol Bioinform Online 17: 11769343211058463, 2021.
41. Ritchie ME, Phipson B, Wu D, Hu Y, Law CW, Shi W and Smyth GK: limma powers differential expression analyses for RNA-sequencing and microarray studies. Nucleic Acids Res 43: e47, 2015.
42. Livak KJ and Schmittgen TD: Analysis of relative gene expression data using real-time quantitative PCR and the 2(-Delta Delta C(T)) method. Methods 25: 402-408, 2001.
43. Mayakonda A, Lin DC, Assenov Y, Plass C and Koeffler HP: Maftools: Efficient and comprehensive analysis of somatic variants in cancer. Genome Res 28: 1747-1756, 2018.
44. Geeleher P, Cox N and Huang RS: pRRophetic: An R package for prediction of clinical chemotherapeutic response from tumor gene expression levels. PLoS One 9: e107468, 2014.
45. Ringnér M: What is principal component analysis? Nat Biotechnol 26: 303-304, 2008.
46. Sherman MH and Beatty GL: Tumor microenvironment in pancreatic cancer pathogenesis and therapeutic resistance. Annu Rev Pathol 18: 123-148, 2023.
47. Moffitt RA, Marayati R, Flate EL, Volmar KE, Loeza SG, Hoadley KA, Rashid NU, Williams LA, Eaton SC, Chung AH, *et al*: Virtual microdissection identifies distinct tumor- and stroma-specific subtypes of pancreatic ductal adenocarcinoma. Nat Genet 47: 1168-1178, 2015.
48. Chakravarthy A, Khan L, Bensler NP, Bose P and De Carvalho DD: TGF-β-associated extracellular matrix genes link cancer-associated fibroblasts to immune evasion and immunotherapy failure. Nat Commun 9: 4692, 2018.
49. Collisson EA, Sadanandam A, Olson P, Gibb WJ, Truitt M, Gu S, Cooc J, Weinkle J, Kim GE, Jakkula L, *et al*: Subtypes of pancreatic ductal adenocarcinoma and their differing responses to therapy. Nat Med 17: 500-503, 2011.
50. Samstein RM, Lee CH, Shoushtari AN, Hellmann MD, Shen R, Janjigian YY, Barron DA, Zehir A, Jordan EJ, Omuro A, *et al*: Tumor mutational load predicts survival after immunotherapy across multiple cancer types. Nat Genet 51: 202-206, 2019.
51. Kang K, Xie F, Mao J, Bai Y and Wang X: Significance of tumor mutation burden in immune infiltration and prognosis in cutaneous melanoma. Front Oncol 10: 573141, 2020.
52. McNamara MG, Jacobs T, Lamarca A, Hubner RA, Valle JW and Amir E: Impact of high tumor mutational burden in solid tumors and challenges for biomarker application. Cancer Treat Rev 89: 102084, 2020.
53. Hayashi A, Hong J and Iacobuzio-Donahue CA: The pancreatic cancer genome revisited. Nat Rev Gastroenterol Hepatol 18: 469-481, 2021.
54. Leng S, Huang W, Chen Y, Yang Y, Feng D, Liu W, Gao T, Ren Y, Huo M, Zhang J, *et al*: SIRT1 coordinates with the CRL4B complex to regulate pancreatic cancer stem cells to promote tumorigenesis. Cell Death Differ 28: 3329-3343, 2021.
55. Li C, Heidt DG, Dalerba P, Burant CF, Zhang L, Adsay V, Wicha M, Clarke MF and Simeone DM: Identification of pancreatic cancer stem cells. Cancer Res 67: 1030-1037, 2007.
56. Marengo A, Forciniti S, Dando I, Dalla Pozza E, Stella B, Tsapis N, Yagoubi N, Fanelli G, Fattal E, Heeschen C, *et al*: Pancreatic cancer stem cell proliferation is strongly inhibited by diethyldithiocarbamate-copper complex loaded into hyaluronic acid decorated liposomes. Biochim Biophys Acta Gen Subj 1863: 61-72, 2019.
57. Babak MV and Ahn D: Modulation of intracellular copper levels as the mechanism of action of anticancer copper complexes: Clinical relevance. Biomedicines 9: 852, 2021.

58. Helgadottir H, Ghiorzo P, van Doorn R, Puig S, Levin M, Kefford R, Lauss M, Queirolo P, Pastorino L, Kapiteijn E, *et al*: Efficacy of novel immunotherapy regimens in patients with metastatic melanoma with germline CDKN2A mutations. J Med Genet 57: 316-321, 2020.
59. Wang P, Guo W, Liu S, Li S, Li J, Ding B, Yin F, Yang Y, Li X, Cao P, *et al*: Novel Pt@PCN-Cu-induced cuproptosis amplifies αPD-L1 immunotherapy in pancreatic ductal adenocarcinoma through mitochondrial HK2-mediated PD-L1 upregulation. J Exp Clin Cancer Res 44: 149, 2025.
60. Gao S, Ge H, Gao L, Gao Y, Tang S, Li Y, Yuan Z and Chen W: Silk Fibroin nanoparticles for enhanced cuproptosis and immunotherapy in pancreatic cancer treatment. Adv Sci (Weinh) 12: e2417676, 2025.
61. Zhang C, Zeng Y, Guo X, Shen H, Zhang J, Wang K, Ji M and Huang S: Pan-cancer analyses confirmed the cuproptosis-related gene FDX1 as an immunotherapy predictor and prognostic biomarker. Front Genet 13: 923737, 2022.
62. Costa A, Kieffer Y, Scholer-Dahirel A, Pelon F, Bourachot B, Cardon M, Sirven P, Magagna I, Fuhrmann L, Bernard C, *et al*: Fibroblast heterogeneity and immunosuppressive environment in human breast cancer. Cancer Cell 33: 463-479.e10, 2018.
63. Huang H, Wang Z, Zhang Y, Pradhan RN, Ganguly D, Chandra R, Murimwa G, Wright S, Gu X, Maddipati R, *et al*: Mesothelial cell-derived antigen-presenting cancer-associated fibroblasts induce expansion of regulatory T cells in pancreatic cancer. Cancer Cell 40: 656-673.e7, 2022.
64. Derynck R, Turley SJ and Akhurst RJ: TGFβ biology in cancer progression and immunotherapy. Nat Rev Clin Oncol 18: 9-34, 2021.



Copyright © 2025 Ge et al. This work is licensed under a Creative Commons Attribution-NonCommercial-NoDerivatives 4.0 International (CC BY-NC-ND 4.0) License.